Research papers

Surface modification of activated carbon with silver nanoparticles for electrochemical double layer capacitors

Amrita Jain [a,*], Monika Michalska [b], Angelika Zaszczyńska [a], Piotr Denis [a]

[a] *Institute of Fundamental Technological Research, Polish Academy of Sciences, Pawiński ego 5B, 02-106 Warsaw, Poland*
[b] *Department of Chemistry and Physico-Chemical Processes, Faculty of Materials Science and Technology, VŠB-Technical University of Ostrava, 17. listopadu 2172/15, 708 00 Ostrava-Poruba, Czech Republic*

ABSTRACT

In the present work, we report the synthesis of surface modified activated carbon (AC). The surface of the activated carbon have been modified by using silver nanoparticles. The synthesis process is simple, cost effective and environment friendly. The modified-AC powders have been characterized by using X-ray diffraction, scanning electron microscopy and surface area and pore size measurements. The electrochemical performance of the prepared materials have been tested by fabricating symmetric configuration of EDLC by using magnesium-ion based polymer electrolytes. The cells have been tested by using cyclic voltammetry, electrochemical impedance spectroscopy and galvanostatic charge-discharge technique. AC with 3 wt% of silver presents best results with specific capacitance of the order of 398 F g^{-1} energy density and power density of 55 Wh kg^{-1} and 2.4 kW kg^{-1} making it an interesting material for supercapacitor application.

1. Introduction

Considering the high power density, quick recharge time, and long life, supercapacitors (SCs) have attracted a lot of attention in recent years [1–4]. They have been utilized in a wide range of areas, such as portable and commercial/household electronics, grid installations, and different forms of transportation (buses, trams, trolleybuses, etc.) [1–4]. The configuration of a supercapacitor device is as simple as conventional capacitors [5,6]. An electrolyte (liquid/solid/gel) is sandwiched between two electroactive electrodes to fabricate a supercapacitor cell [5,6]. On the basis of the types of electrode materials used and the charge storage mechanism, it is classified into two types; (a) electrochemical double layer capacitors (EDLCs) in which large surface area carbonaceous types of materials are used and the charge storage mechanism is electrostatic in nature; and (b) pseudocapacitors, in which conducting polymers and electroactive oxides are used and fast faradic charge transfer reaction gives rise to pseudocapacitance [1–8].

Carbon-based materials have been applied as a first materials in electrodes in lithium-ion batteries and supercapacitors due to their natural abundance, low cost, high electrical conductivity, and significant capacitance related to their high specific surface area [9–12]. Different forms of carbon have been tested as electrode materials in SCs

such as: carbon nanotubes (CNT), graphene, carbon aerogel, carbon nanofibers (CNF) and activated carbon (AC) [9–22]. Up to now, activated carbons are attractive electrode materials for an EDLC capacitor from the economic point of view and the possibility of obtaining a well-developed specific surface area of ca. 2500 $m^2 g^{-1}$ with a controlled pore size distribution and also because of its surface chemistry which can be easily modified to improve its performance by surface modification via; post treatment of carbon materials with reactive heteroatom sources or by making composites of carbon with either metal oxide materials or conducting polymers [21–25]. Yumak et al. [23] prepared the composites of activated carbon with MnO_2 as well as with NiO using hydrothermal and precipitation techniques. The authors discovered that adding MnO_2 and NiO to activated carbon-based supercapacitors increased their specific capacitance by 50 % and 150 %, respectively [23]. This behavior was ascribed to the pseudocapacitive effect of MnO_2 and NiO, as well as the effect of oxygen-containing surface functional groups derived from the composite synthesis process [23]. The authors also claimed that the surface functional groups, surface area, and thermal stability of achieved composite materials, as well as the electrochemical parameters of fabricated supercapacitors, were all affected by the synthesis procedure [23]. Vijayan and co-authors [26] proposed the easy technique to modify activated carbon material with thin

---

* Corresponding author.
E-mail address: ajain@ippt.pan.pl (A. Jain).

manganese oxide and they revealed that the best results of a two-fold increase in the specific capacitance in 1 M Na_2SO_4 electrolyte delivered material of composition: 10 wt% Mn_2O_3@AC [26]. The authors tested their material as a symmetric supercapacitor with 1 M Na_2SO_4 electrolyte and the material had an energy density of 31 Wh kg^{-1}, power density of 4.8 kW kg^{-1} [26]. A redox reaction was utilized to deposit the RuO_2 nanoparticles on the microporous carbon surfaces by Y. Zhang and S.-J. Park [27]. The material of composition 9 wt% RuO_2@AC had a specific capacitance of 510 Fg^{-1}, at a current density of 1 Ag^{-1}, and the capacitance retention was 87 % at a current density of 1 Ag^{-1} after 3000 cycles [27]. A thin metallic cobalt film was deposited on porous carbon (PC) by Vijayan et al. [28]. The modified material (10 wt% Co@PC) was examined as an electrode for aqueous alkaline supercapacitors in 1 M Na_2SO_4 and lithium-ion capacitors using an ionic liquid (1 M $LiPF_6$). The specific energy and specific power of the aqueous alkaline supercapacitor built with the Co-modified porous carbon electrode were nearly 10 times higher than those prepared with the pure porous carbon electrode [28]. The composite made of void-size-matched hierarchical 3D titania flowers in porous carbon (TiO_2@AC) was synthesized by the hydrothermal method [29]. The composite material was tested in 1 M Na_2SO_4 electrolyte and the constructed electrode in SCs delivered 143 F g^{-1} at 1 A g^{-1}, energy density of 28 W h kg^{-1}, power density of 4.8 kW kg^{-1}, and the stability was 95 % at a current density of 1 Ag^{-1} after 5000 cycles [29]. Hydrothermal synthesis was utilized by Mohamed et al. [30] to obtain composite of ZnO@activated carbon. The material was examined as supercapacitor electrode material in acidic (H_2SO_4) and alkaline (KOH) electrolytes [30]. The specific capacitance of 667 Fg^{-1} of ZnO@activated carbon composite showed better capacitance performance when compared to pristine AC (355 Fg^{-1}) [30]. After 3000 cycles, the material maintained 90 % of its specific capacitance [30]. The goal of as-presented works was to show that each modification with metallic, metal oxide particles, or conductive polymers or other carbon materials positively affect the electrochemical performances while the material was tested as supercapacitor electrode material. Moreover, the researchers also claimed that after the modification the achieved composites materials possessed higher specific surface area and porosity which resulted to increase desired parameters for SC applications, like specific capacitance, energy, and power density. Considering the above-mentioned facts in the present work, the surface of the activated carbon has been modified by using silver (Ag) particles, these particles will enhance the electrical charge transfer which finally improves the electrochemical performance. Kim et al. reported the effect of modifying the graphite nanofibers and PANI electrode with Ag nanoparticles and found that silver significantly improved the specific surface area along with the electrochemical utilization of electrodes [31].

Along with the electrode materials, electrolytes are also the important component of energy storage device like lithium-ion batteries or supercapacitors [32–35]. Because of their different physical and chemical properties, they play differently at the interface with different electrodes and hence they possess different electrochemical characteristics of the device. Though aqueous electrolytes like KOH, H_2SO_4, NaCl etc. have advantages like high ionic conductivity, environmentally friendly, cost effective, non-flammability etc. but the main drawback is its limited electrochemical stability range and unsafe handling [35]. In order to find a mid-way, gel polymer electrolytes (GPEs) are excellent substitute due to their acceptable ionic conductivity and solid like dimensional stability. The most commonly used polymers to entrap the liquid electrolytes are poly(vinyl alcohol) (PVA) [36,37], poly(vinyl pyrrolidone) (PVP) [38], poly(methyl methacrylate) (PMMA) [39], poly (vinylidene fluoride-co-hexafluoropropylene) (PVdF-HFP) [40,41] etc. Out of these polymers, PVdF-HFP is used abundantly because of its good mechanical stability, thermal stability and chemical resistivity.

In the present work, surface modified activated carbon with different weight percentage of silver particles were used as an electrode material and free standing gel polymer electrolyte using PVdF-HFP as host polymer and magnesium perchlorate ($Mg(ClO_4)_2$) as salt were used.

Modified activated carbon has been characterized by using different techniques like BET, XRD and SEM, EDLC cell has been fabricated by using surface modified activated carbon and GPE. The performance characteristics of EDLC cells have been evaluated by impedance spectroscopy, cyclic voltammetry (CV) and galvanostatic charge-discharge measurements.

2. Experimental details

2.1. Preparation of surface modified activated carbon

The nanocomposites of activated carbon (AC) (Activated charcoal pure p.a., CHEMPUR) with 1, 3 and 5%wt. Ag were fabricated by a facile chemical low-temperature route. In the first step, $AgNO_3$ (used as a Ag source, purchased as a pure from Lachema) was dissolved in ethanol solution (EtOH, 96 %, Merci) in the weight ratio Ag/AC: 0.01, 0.03, and 0.05, respectively. This process was carried out at room temperature. In the second step, the AC powder was added to the $AgNO_3$-EtOH-H_2O solution. The as-prepared mixture was magnetically stirred for a few hours to obtain a black homogeneously dispersed suspension. Afterwards, the suspension was kept in an ultrasonic water bath cleaner for 1 h from 25 to 60 °C. Each suspension was overnight air-dried at 60 °C and then at 150 °C for a few hours. To obtain a fine powder, the AC/n-Ag (n-denotes: 1, 3 and 5%wt. Ag) nanocomposites were grinded in an agate mortar for 1 h. The prepared samples from hereafter called as ACAG1, ACAG3, ACAG5.

The structure of the prepared carbon material composites were characterized by using X-Ray powder diffraction (XRD) by using Bruker D8 Discover Diffractometer equipped with CuKα ($\lambda_{XRD} = 1.542$ Å) radiation source and by the confocal Raman spectrometer (Renishaw inVia) equipped with a charge-coupled device (CCD) camera and a continuous wave diode pumped Nd:YAG laser working at λ = 532 nm, respectively. Morphological studies of ACAG1, ACAG3 and ACAG5 were carried out by field emission scanning electron microscopy using the instrument SEM/FIB-Zeiss Crossbeam 350, Germany. A thermal analyzer DSC SDTQ600, DSC TGA Instrument was used to study the thermal stability of ACAG composite materials from 30 °C to 900 °C with a heating rate of 10 °C min^{-1} under Argon flow 20 ml min^{-1}. The specific surface areas of the carbon materials were measured with the AutoSorb IQ, Quantachrome, USA under nitrogen flow. The pore size distribution curves were obtained by using DFT model.

2.2. Fabrication and characterization of EDLC cells

GPE films were prepared by using standard solution cast technique. The details of the preparation and characterization of the polymeric films were described elsewhere [42]. The capacitor electrodes were prepared in the form of flexible electrodes. All the three activated carbon powders (ACAG1, ACAG3, ACAG5) were grinded for 30 min individually in pestle mortar to get a uniform and fine powder. PVdF is used as a binder in the ratio of 90:10 (*w/w*). PVdF and acetone (solvent) was magnetically stirred for 30 min and later a slurry was performed. The slurry was casted over carbon cloth (AvCarb, USA). The prepared electrodes were airdried at 80 °C before using them to fabricate the EDLC cells. The mass loading of active material was in between 0.39 and 0.43 mg cm^{-2}. To fabricate the EDLC cell, GPE were sandwiched between the symmetrical electrodes. Three EDLC cell (Cell A-C) were fabricated by using ACAG1, ACAG3, ACAG5 respectively. All the cells were electrochemically characterized by using Biologic VMP3 (Seyssinet-Pariset, France) electrochemical workstation.

3. Results and discussion

3.1. Structural studies and morphology data (XRD, Raman spectroscopy, SEM, BET and TGA)

The XRD pattern of activated carbon (AC) material, pure and decorated with 1, 3 and 5 % wt. Ag is presented in Fig. 1. The AC amorphous peaks are situated at around 26° and 43° [12]. There are also visible crystal peaks for pure AC, coming from graphite or other hexagonal carbon structures. As shown in Fig. 1, the diffractograms of materials with Ag present, feature two characteristic peaks at 2θ angles of: 38.1, and 44.3° for CuKα radiation (λ = 1.542 Å), corresponding to the crystal planes (111) and (200), respectively. That two reflections represent the metallic Ag phase (COD 9008459). Crystal peak at 32.1° can be ascribed to the nanocrystalline silver, (122) plane [43]. The peaks intensity growth with the increase of Ag content from 1 to 5 % wt. was observed and indicated that metallic Ag nanoparticles were successfully deposited on the surface of activated carbon material. These results were further confirmed by SEM analysis as well as have found positive effect while electrochemical performances were evaluated. According to the Ag single crystallites size analysis, they are supposed to be below 1 nm, and the Ag particles observed in SEM, consisting of many crystallites, have an average size of 10 nm.

Raman spectroscopy was utilized to get more information about the structural features of pristine AC material and one selected sample of AC modified with 3%wt. Ag. The obtained results are presented in Fig. 2. The crystal structure of AC powders remained unchanged after Ag modification, as expected. The Raman spectra feature four well-defined bands at 1340, 1580, 2690, and 2942 cm^{-1}, which correspond to the D, G, 2D, and D + G bands of typical graphitic materials, respectively [12]. Attributed to the prevalence of sp^3 hybridization in the carbon structure and the E_{2g} phonon vibrations of the sp^2 carbon atoms, the D and G bands are related with the A_{1g} vibrational mode of the disordered carbon structure [12,44]. The scattering of phonons at the zone boundary (K point) causes the 2D mode, which is a second-order vibration of the G mode [12,43]. The combination of D and G peaks can be induced by the presence of various defects in the graphitic structure [12,44]. It is also possible to establish the "degree of graphitization", which informs on the crystallinity level of carbon materials, by comparing the intensity ratios of the D to G bands (I_D/I_G) [12,44]. For the AC and ACAG3 samples, the estimated I_D/I_G values are 1.100 and 1.093, respectively. These calculations of the intensity ratios revealed that both of the carbon structures studied: pristine AC and AC modified with 3%wt. Ag materials are quite disordered. The AC material modified with 3%wt. Ag has a little higher degree of graphitization in comparison to pristine AC
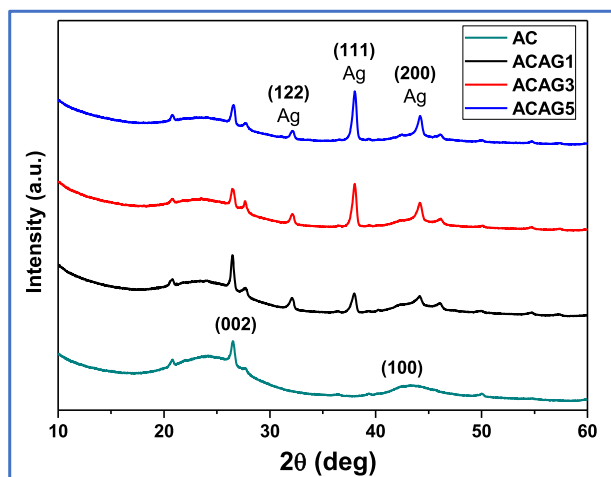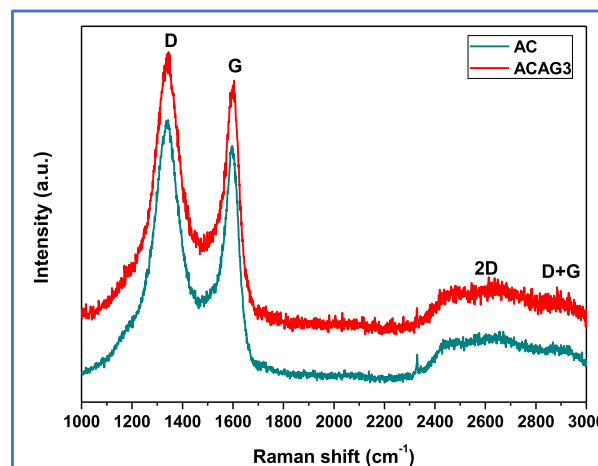

Fig. 2. Raman spectra of pristine AC material and modified with 3%wt. Ag.

material.

The surface micrographs of silver modified activated carbon (ACAG1, ACAG3, ACAG5) are illustrated in Fig. 3. As can be seen from the morphologies that deposition of silver nanoparticles were confirmed and they were observed as a small balls (less than 10 nm). Owing to special morphology which represent activated carbon material we could suppose that the small balls of metallic Ag are placed between the carbon nanosheets. Also, from the morphology of ACAG3 it can be seen that the small pores are developed which provides the facile accessibility for electrolyte ions, which are beneficial in forming capacitive interface with gel polymer electrolytes.

The thermal behaviors of ACAG1, ACAG3, and ACAG5 samples were examined from 30 to 900 °C with a heating rate 10 °C min^{-1} in argon atmosphere (Fig. 4). The three-stage loss of weight is observed for all analyzed samples. First occurs from the temperature 30 to ca. 150 °C and is related to the evaporation of the residual water (ca. 9 %) as well as accompanies the decomposition processes of carbon material into non-condensable gases such as CO, CO_2, CH_4, H_2, and others [45]. The weight loss observed in the second stage, between ca. 200 °C and 600 °C, is attributable to the heat degradation of raw materials. These reactions are accompanied by further chemical changes such as dehydration, degradation, and condensation, all of which result in the loss of aliphatic character, increasing aromaticity and releasing gases simultaneously [45]. At the third-stage the significant effect of weight loss of 35 %, 25 %, and 45 % was observed in the temperature range from 600 °C to 900 °C for samples: ACAG1, ACAG3, and ACAG5, respectively. That stage displays the final weight loss, which indicates that the active sites have completely reacted as well as being a measure of the synthesized material's thermal stability [45].

N_2 adsorption-desorption isotherms have been recorded for ACAG1, ACAG3 and ACAG5 powders and are typically shown in Fig. 5(a–c). As can be seen from the isotherms, all the samples shows an initial N_2 uptake followed by a gradual increase. All isotherms shows type II pattern (IUPAC nomenclature) in which at very low pressures, the micropores are fill with the nitrogen gas. At the knee, formation of monolayer starts and multilayer formation takes place at the medium pressure. At the higher pressures, usually capillary condensation takes place [46]. Table 1 summarizes the values of various parameters estimated from this studies. The 45 micropore volumes (V_{micro}) of all the samples are estimated from t-plot method and are tabulated in Table 1. As can be seen from the values, ACAG3 shows the highest surface area with low pore size, but as the percentage of silver increases, it leads to decrease in microporosity and increase of mesoporosity which leads to decrease in the specific surface area as well. All the material shows small hysteresis in desorption branch which confirms the presence of small amount of mesopores along with micropores. This trend is well-
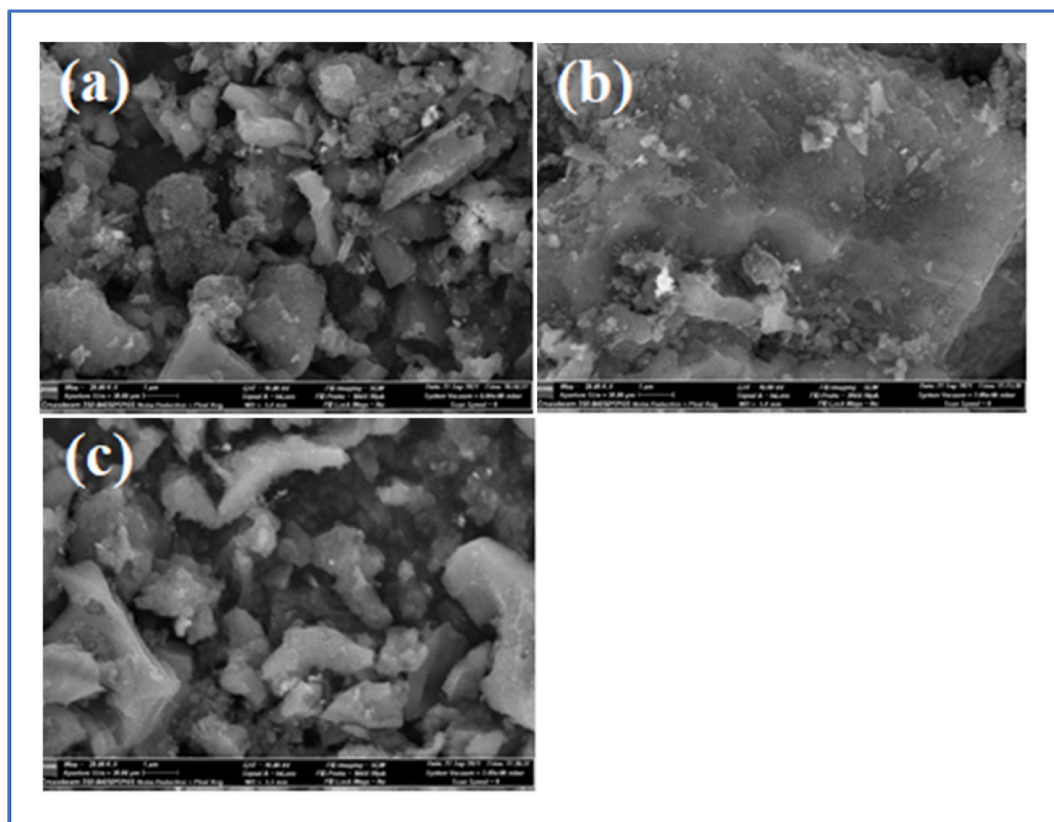

Fig. 1. XRD spectra of AC materials modified with 1, 3 and 5%wt. Ag.

Fig. 3. SEM images obtained at 20.000 magnification of: (a) ACAG1, (b) ACAG3, (c) ACAG5 samples.
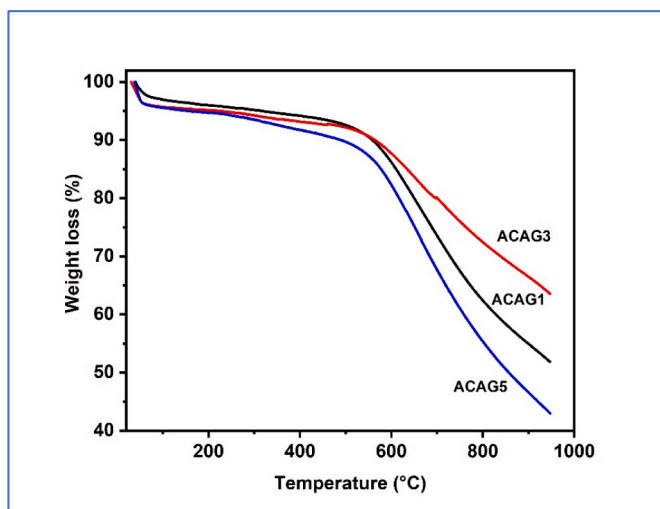

Fig. 4. TGA curve of ACAG composites modified with 1, 3 and 5%wt. Ag.

connected with electrochemical studies (discussed later) as well. The pore size distribution for each sample is shown in the inset of the respective figures, it has been calculated by using Barret-Joyner-Halenda (BJH) method analysis of desorption branch [47–50]. It has been observed that the prepared compositions show the highest concentration of pores in between 0.5 nm to 2.3 nm but in case of ACAG5, the pore width is broader as compared to other two compositions and hence this larger pores created was blocked by silver particles. These results are also in synchronization with electrochemical results. Overall, we observed the ACAG3 has the maximum surface area with good and optimized pore size distribution.

3.2. Electrochemical studies

Symmetrical configuration of the EDLC cells with four types of electrode materials with polymer gel electrolytes are given below:

Cell#A: ACAG1|GPE|ACAG1
Cell#B: ACAG3|GPE|ACAG3
Cell#C: ACAG5|GPE|ACAG5
Cell#Ref: Pure AC|GPE| Pure AC

As mentioned above, four kind of EDLC cells were fabricated by using surface modified activated carbon materials and the results has been compared with pristine activated carbon as well. GPE in the present study is PVdF-HFP-PC-Mg(ClO$_4$)$_2$. Comparative impedance measurements, CV and GCD measurements have been carried out and discussed in this section.

Fig. 6a shows the room temperature cyclic voltammograms obtained for cell #A-#C, the CV plot of Cell#Ref is shown in supplementary material (Fig. S1). The results shows the significant contribution of silver particles. A non-symmetric charge discharge profile of CV of the electrochemical double layer is also verified. Ideally the cyclic voltammograms of the electrochemical double layer cell is in the form of symmetrical rectangular shape [51]. As can be seen from the curves that with the increase in the percentage of silver, there is the loss in the symmetry and it might be due to the reversible pseudo-faradic reactions and the redox peak becomes prominent in case of 3 and 5 wt% and in the case of pure and 1 wt% of silver the redox peaks are almost absent. Interestingly there is an increase of the electric double layer capacitance in the voltametric profiles from 0 wt% to 3 wt% and after that there is sharp degradation of the capacitance values. It might be due to the blockage of pores because of the increased amount of silver particles, also BET studies confirms that the surface area of 5 wt% of silver modified material is low and pore size is large as compared to rest of the materials. The trend is consistent with GCD and impedance studies also and are discussed in the following section. Up to 3 wt% silver
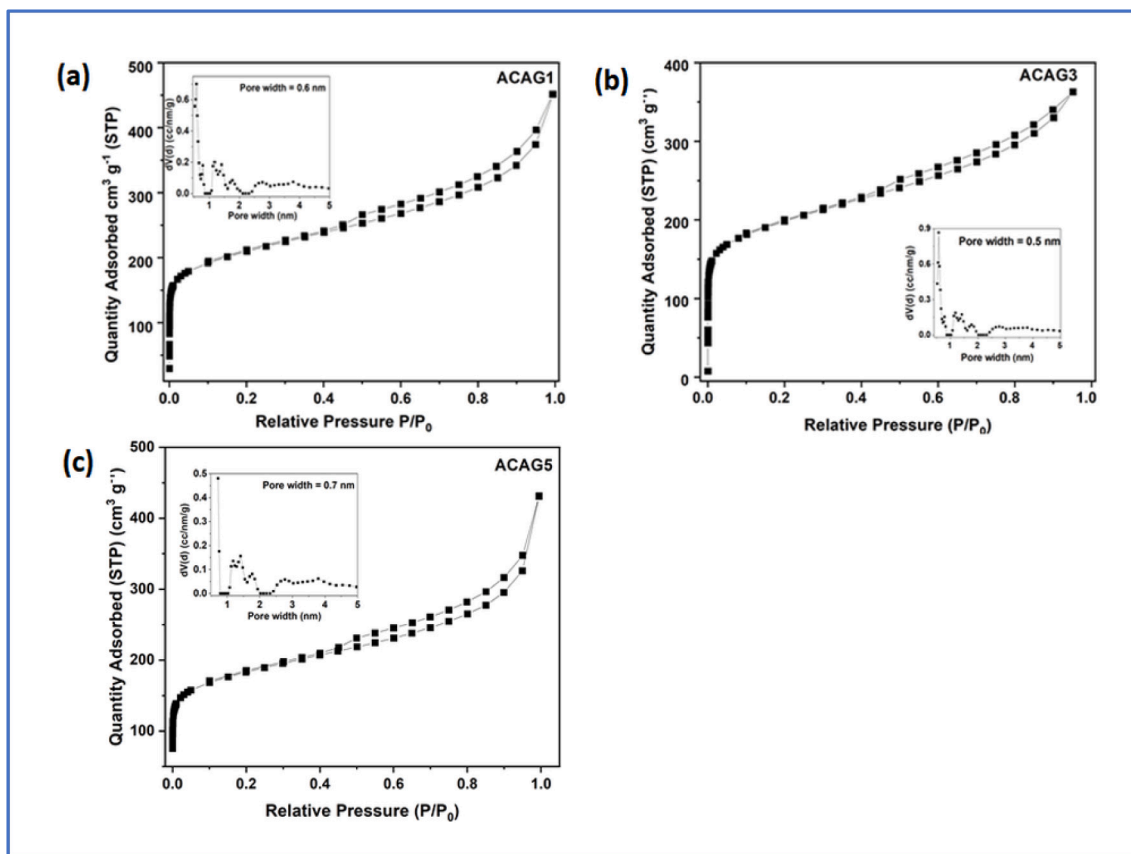
Fig. 5. N_2 adsorption-desorption isotherms and inset; pore size distribution spectra of: (a) ACAG1, (b) ACAG3, (c) ACAG5.

Table 1
Parameters estimated from N_2 adsorption-desorption measurements.

Sample	SSA (BET) $m^2\,g^{-1}$	V_{micro} ($cm^3\,g^{-1}$)	D_{avg} (nm)
ACAG1	743.2	0.60	0.6
ACAG3	824.7	0.49	0.5
ACAG5	679.9	0.53	0.7

nanoparticles plays a positive role by enhancing the exposed surface area so that the most effective electrochemical double layer process takes place. The CV curves were recorded at the scan rate of 5 mV s^{-1} in the potential range of 0 V to 1.0 V. The capacitance values calculated by using CV technique (Eq. (1)) [49] for cell #A-#C are 231.5 F g^{-1}, 362.5 F g^{-1} and 59.6 F g^{-1} respectively.

$$C_s = \int IdV \bigg/ s \times \Delta V \times m \qquad (1)$$

where, s is the scan rate, V is the voltage range and m is the mass of the active material used in single electrode.

As can be seen that there is a significant drop of capacitance value for cell #C in which 5 wt% Ag is used for surface modification. Fig. 6b depicts the variation of capacitance as a function of scan rate for capacitor cell #A-#C. As can be seen from the plot, at lower scan rate there is a slight decrease in the values of capacitance, after that almost
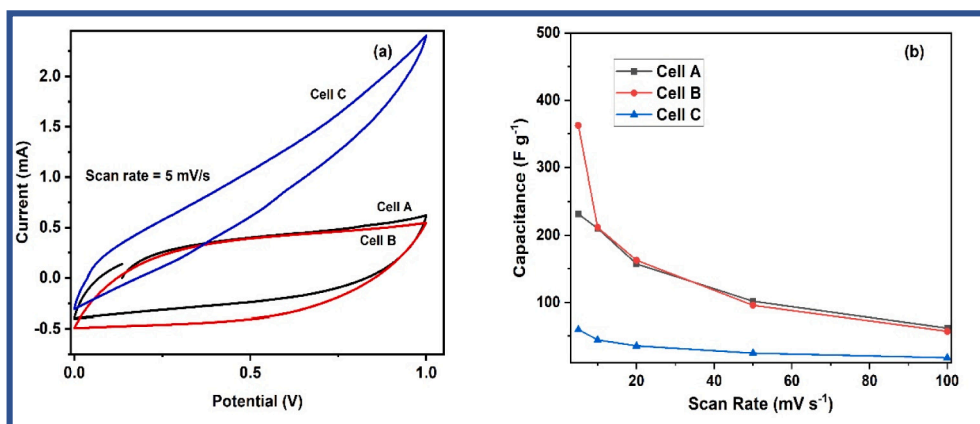

Fig. 6. (a) Comparative cyclic voltametric curves of cell #A-#C recorded at a scan rate of 5 mV s^{-1} and (b) Variation of specific capacitance of cell #A-#C as a function of scan rate.

stable and constant capacitance values has been observed even for higher scan rates like 100 mV s^{-1} which shows the fast ion switching behavior at the interface of the electrode and electrolyte. This confirms the suitability of gel polymer electrolyte for the application of EDLCs.

Impedance spectroscopy also called as electrochemical impedance spectroscopy (EIS) studies are carried out to find insight information about the capacitor cells such as bulk resistance, charge-transfer resistance, diffusion phenomenon at the electrode and electrolyte interfaces and finally the charge storage in terms of specific capacitance [50]. Fig. 7a shows the impedance (Nyquist) plots for the cells #A-#C with the magnesium ion based gel polymer electrolyte recorded in the frequency range from 200 kHz to 1 mHz at room temperature (25 °C).

The EIS plot of Cell#Ref is provided in the Supplementary material (Fig. S2) for comparison. Impedance plots of any supercapacitor cells are divided into three regions, capacitance at lower frequencies, resistance at high frequencies and ion penetration effect of electrode materials in the middle frequency region. The vertical line parallel to the imaginary axis of the impedance plot shows the ideal capacitor behavior. It can be seen from the plots that all the cells shows steep rising in the lower frequency region which confirms the capacitive nature of all cells. In the high/middle frequency range, the semicircular spur is also observed from which the information of bulk resistance, charge transfer resistance at the electrode electrolyte interface can be obtained. The difference in the diameter of the semicircles may be associated to the functional group or the influence of silver particles on the surface of activated carbon. Similar to CV results, impedance results also shows the same pattern, up to 3 wt% of silver particles, the values of capacitance increased and for 5 wt% it significantly dropped and the resistance value increased which clearly confirms the blockage of pores of material when it is modified with 5 wt%. The values of bulk resistance R_b, charge transfer resistance R_{ct}, overall resistance R and capacitance C measured at a frequency of 1

mHz are summarized in Table 2. The capacitance values were calculated by using Eq. (2) [49].

$$C = \frac{2}{2\pi f m |Z''|} \qquad (2)$$

where, m is the mass of the single electrode, f is the frequency and Z'' is the value of imaginary impedance typically at 1 mHz.

The rate performance of the capacitor cell B has been evaluated from impedance analysis following the Miller's approach [51] by plotting the Bode plots of impedances (Z' and Z'' vs. frequency) which are illustrated in Fig. 7b. From these plots, the value of the characteristic resonant frequency (f_0) can be obtained, it is that intersecting point where real and imaginary values are equal. This frequency is also known as response frequency where real and imaginary parts of impedance has a phase difference of ~45° and the reciprocal of this frequency is called as response time (τ_0). Response time is basically the time which is taken by electrolyte ions to adsorb and desorb in the pores of the electrode material (ACAG in the present case). Further, the response frequency of the

Table 2
Electrical parameters of Cell #A-#C from impedance analysis.

Cells	R_{ct} (Ω cm^2)	R_b (Ω cm^2)	1 mHz		
			R (Ω cm^2)	C	
				(mF cm^{-2})[a]	(F g^{-1})[b]
#A	4.2	42.4	600.8	188.7	180
#B	3.1	31.5	124.3	344.3	229.6
#C	5.5	52.5	453.1	112.6	56.3

[a] Overall capacitance of cell.
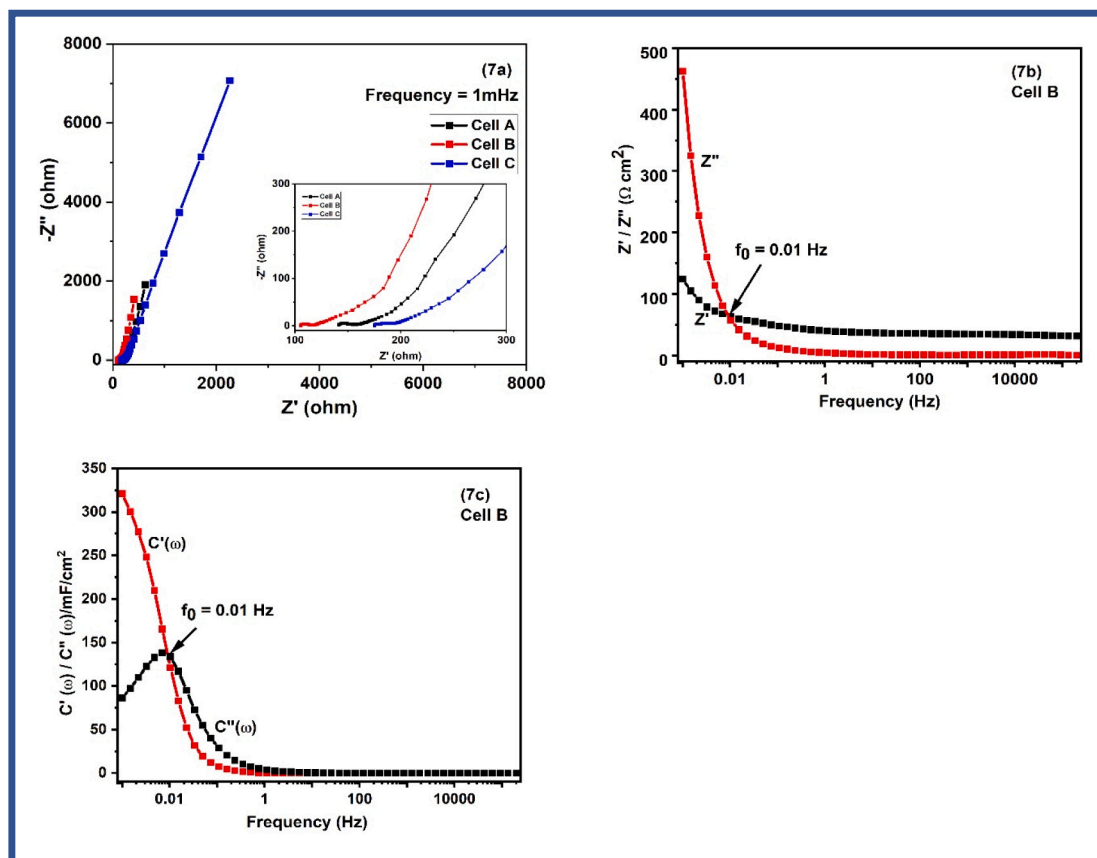[b] Single electrode specific capacitance of the cell.

Fig. 7. (a) EIS plots of EDLC cell #A-#C. Expanded representation of EIS plot in high/mid frequency region is shown in inset, (b) real and imaginary impedances versus frequency (c) real and imaginary capacitances versus frequency.

cell B recorded from Miller Bode plots has also been estimated by using Taberna plot (real and imaginary capacitance vs. frequency) and is shown in Fig. 7c. It has been observed that the response frequencies and hence response times are in good alignment with the values obtained from Miller plots. The resonant frequency for cell B is 0.01 Hz and response time (τ_0) is 14.2 s. The cell has lower response frequency and higher response time due to the presence of silver ions at the interface of the cell.

To supplement the results obtained from EIS and CV, galvanostatic charge-discharge (GCD) studies were also performed to evaluate the rate performance of the surface modified carbon materials. Fig. 8(a) depicts the GCD curve of cell #A-#C at the current density of 1.0 mA cm^{-2} and in a potential window of 0 to 1.0 V. All the three cells shows the curved nature of charge-discharge patterns. The non-linear pattern in GCD curves while charging and discharging are owing to the redox peaks which was observed in CV studies as well. The reversible redox reactions at the interface because of which plateau regions appears during charge-discharge are responsible for higher values of capacitance [52]. The capacitance was calculated using the discharge branch excluding the ohmic drop. For comparison GCD curve of Cell#Ref is provided as Fig. S3 in supplementary information. In GCD studies also, same trend has been observed capacitance values were gradually increased from 0 wt% to 3 wt% of silver particles and later it sharply decreased in case of 5 wt%. The discharge specific capacitance C_d from non-linear discharge profile has been calculated by using the Eq. (3) [49]:

$$C_d = \frac{4i \int V dt}{m \times V^2}\bigg|_{V_i}^{V_f} \qquad (3)$$

where, i is the current density, m is the mass of active material of single electrode, $\int V dt$ is the area under the discharge curve, V is the maximum operating voltage and V_i and V_f are the initial and final values of voltages on the GCD curves. Long term cycling efficiency is another studies by which stability of cells are estimated [50]. Continuous charge-discharge cycles were carried out for 10,000 cycles at the current density of 1 mA cm^{-2} between 0 and 1.0 V. The cyclic testing was performed for the best cell (cell B in the present case) and is shown in Fig. 8b. As can be seen from the figure, there is a decrease in early stage of cycling, it may be because of the loss of charges resulting from adsorption of ions at the electrode-electrolyte interface or accumulation of ions to form ion pairs in the charge-discharge cycling process [53]. Nevertheless, the cell B was stable up to 10,000 cycles after initial decrease in the capacitance values. As can be seen from pattern the capacitance values of cell B shows ~2 % of fading in the beginning is possibly because of the irreversible storage components of electrolyte and later it is consistent because of the proper accessibility of and non-modified pore reachability for electrochemical redox reactions. The results shows the stable cyclic performance of the capacitor cell B. The variation of specific discharge capacitance of the cell as a function of applied current density by using GCD technique is shown in the inset of Fig. 8b. As can be seen from the figure that capacitance gradually increased till 1.4 mA/cm^2 but later it started decreasing with increasing current density which confirms the moderate rate capability of the cell.

To get further insight, SEM images with EDX pattern of cycled ACAG3 electrodes are also carried out and are shown in Fig. 8(c) and EDX pattern are shown in inset of Fig. 8c. It can be that even after 10,000 cycles there is no apparent difference between the morphology of before cycling samples (Fig. 3b) and after cycling samples (Fig. 8c) indicating the stability of ACAG samples. However, in the images, we can see some spheres which may be are from electrolyte materials, may
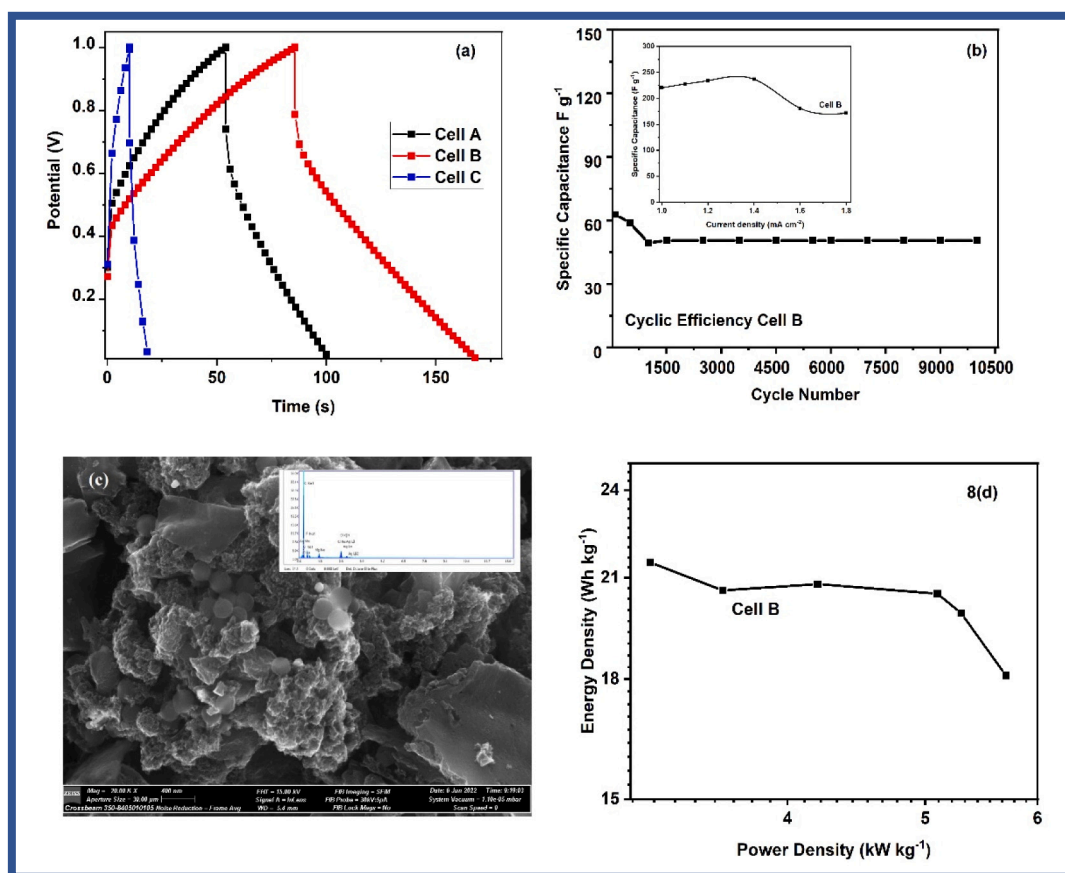

Fig. 8. (a) GCD curves of cell #A-#C recorded at current density of 1 mA cm^{-2} in between 0 and 1.0 V, (b) Specific capacitance of cell #B versus charge discharge cycles measured at constant current density of 1 mA cm^{-2} (c) SEM image and EDX spectra of ACAG3 electrode after cycling.

be some traces of Mg salt or polymer. From EDX spectra, it is also cleared that the ACAG sample after cycling contains traces of Mg, F, O etc. which are because of the interaction of electrode and electrolyte material during electrochemical testing leading to the decrease in the number of mobile ions within the electrolyte and demeriting the performance of device [53].

To make it more clear, the repetition of the specific capacitance after cycling, ac impedance was also carried out after 10,000 cycles and the plot is shown in supplementary Fig. S4. Before cycling, the values of bulk resistance, charge transfer resistance are only 31.5 and 3.1 Ω cm^2 respectively showing the high conductivity and good compatibility between electrode and electrolyte material but after cycling bulk resistance is same 31.6 Ω cm^2 but charge transfer resistance increased to 24.4 Ω cm^2, this confirms that decay in the capacitance storage is due to charge transfer resistance, electrolyte ions might stuck into electrode leading to decrease in number of free ions, additionally this stuck ions might also produce repulsive force among other ions hindering the ion adsorption in electrode electrolyte interface and hence increasing R$_{ct}$ [53].

The specific energy of the cell #A-#C has been calculated by using the expression E = $\frac{1}{2}$ C$_d$V^2, and the power density of the cells were calculated by using $P = E/\Delta t$, where Δt is the discharge time in the cells [42]. The values of discharge capacitance, energy density and power density are summarized in Table 3. The Ragone plot (variation of specific energy E versus effective power density) of cell B has been evaluated at different current densities; 1.0 mA/cm^2 to 1.8 mA/cm^2 and is shown in Fig. 8(d). The energy and power density lies in between 3.0 and 5.8 Wh kg^{-1} and 18.0 to 21.5 kW kg^{-1} respectively. These values are found to be comparable than other carbon-based supercapacitors which are reported in the literature [54–58].

Similarly like cyclic voltammetry and electrochemical impedance spectroscopy, GCD also showed the same pattern, the capacitance values, energy density and power density gradually improved from 0 wt % to 3 wt% and for 5 wt% of silver particles it significantly dropped, it might be because of the blockage of the pores or the incompatibility of pores of electrode material with reference to electrolyte.

4. Conclusions

Surface modified activated carbon in which the modification was done by silver particles were successfully synthesized and investigated as electrode materials for electrochemical double layer capacitors by using magnesium ion based gel polymer electrolytes. The process of surface modification was simple, cheap and safe as well. The modification method allowed the deposition of metallic silver in nano-size dimension. The modification was confirmed by SEM, XRD, Raman, and BET analyses. From the electrochemical studies, modification with 3 wt% of silver was optimized for energy storage application. This interesting and inimitable architecture of highly porous carbon materials provides a facile and low cost opportunity for developing electrochemical double layer cells. Despite of low quantity of silver deposited there was significant increase in the properties of the material. Electrochemical studies of ACAG3 shows excellent results having specific capacitance of 398 F g^{-1} with energy density and power density of 55 Wh kg^{-1} and 2.4 kW kg^{-1}. The cell showed the stable performance up to 1500 GCD cycles. Combining all the above results, ACAG3 can be considered as a potential candidate for supercapacitor applications.

CRediT authorship contribution statement

Amrita Jain: Conceptualization, Methodology, Validation, Investigation, Resources, Data curation, Writing—original draft preparation, Writing—review and editing, Supervision, Project administration, Funding acquisition. **Monika Michalska:** Methodology, Validation, Formal analysis, Investigation, Writing—original draft preparation,

Table 3
Charge-discharge characteristics of EDLC cell #A-#C at constant current density of 1 mA cm^{-2}.

Cells	Discharge capacitance (C$_d$) [F g^{-1}]	Energy Density (E$_d$) [Wh kg^{-1}]	Power Density (P$_d$) [kW kg^{-1}]
A	237.5	32.9	2.5
B	398.1	55	2.4
C	40.1	5.6	2.2

Writing—review and editing, Visualization, Project administration, Funding acquisition. **Angelika Zaszczyńska:** Investigation, Writing—review and editing. **Piotr Denis:** Writing—review and editing, Investigation, Experiments.

Declaration of competing interest

The authors declare the following financial interests/personal relationships which may be considered as potential competing interests:

Amrita Jain reports financial support was provided by National Centre for Research and Development. Monika Michalska reports a relationship with Ministry of Education Youth and Sports of the Czech Republic that includes: employment.

Data availability

Data will be made available on request.

Appendix A. Supplementary data

Supplementary data to this article can be found online at https://doi.org/10.1016/j.est.2022.105367.

References

[1] A. González, E. Goikolea, J.A. Barrena, R. Mysyk, Review on supercapacitors: technologies and materials, Renew. Sust. Energ. Rev. 58 (2016) 1189–1206.
[2] A. Muzaffar, M.B. Ahamed, K. Deshmukh, J. Thirumalai, A review on recent advances in hybrid supercapacitors: design, fabrication and applications, Renew. Sust. Energ. Rev. 101 (2019) 123–145.
[3] P. Sharma, T.S. Bhatti, A review on electrochemical double-layer capacitors, energy conversManag. 51 (2010) 2901–2912.
[4] F. Bu, W. Zhou, Y. Xu, Y. Du, C. Guan, W. Huang, Recent developments of advanced micro-supercapacitors: design, fabrication and applications, npj Flex Electron 4 (2020) 31.
[5] S. Jha, M. Velhal, W. Stewart, V. Amin, E. Wang, H. Liang, Additively manufactured electrodes for supercapacitors: A review, Appl. Mater. Today 26 (2021) 101220.
[6] K.K. Patel, T. Singhal, V. Pandey, T.P. Sumangala, M.S. Sreekanth, Evolution and recent developments of high performance electrode material for supercapacitors: A review, J. Energy Storage 44 (2021) 103366.
[7] D.P. Chatterjee, A.K. Nandi, A review on the recent advances in hybrid supercapacitors, J. Mater. Chem. A 9 (2021) 15880–15918.
[8] P. Simon, Y. Gogotsi, Materials for electrochemical capacitors, Nat. Mater. 7 (2008) 845–854.
[9] A.G. Pandolfo, A.F. Hollenkamp, Carbon properties and their role in supercapacitors, J. Power Sources 157 (2006) 11–27.
[10] C.-F. Liu, Y.-C. Liu, T.-Y. Yi, C.-C. Hu, Carbon materials for high-voltage supercapacitors, Carbon 145 (2019) 529–548.

[11] S. Saini, P. Chand, A. Joshi, Biomass derived carbon for supercapacitor applications: review, J. Energy Storage 39 (2021), 102646.

[12] A. Jain, M. Ghosh, M. Krajewski, S. Kurungot, M. Michalska, Biomass-derived activated carbon material from native European deciduous trees as an inexpensive and sustainable energy material for supercapacitor application, J. Energy Storage 34 (2021), 102178.

[13] J. Han, J.S. Chae, J.C. Kim, K.C. Roh, Facile preparation of composite electrodes for supercapacitors by CNT entrapment into carbon matrix derived from pitch at a softening point, Carbon 163 (2020) 402–407.

[14] J.P. Mensing, T. Lomas, A. Tuantranont, Ammonia strengthened graphene/CNT-wrapped polyaniline-nanofiber composites loaded with palladium nanoparticles for coin cell supercapacitors, Electrochim. Acta 263 (2018) 17–25.

[15] V.D. Nithya, A review on holey graphene electrode for supercapacitor, J. Energy Storage 44 (2021), 103380.

[16] M. Xu, A. Wang, Y. Xiang, J. Niu, Biomass-based porous carbon/graphene self-assembled composite aerogels for high-rate performance supercapacitor, J. Clean. Prod. 315 (2021), 128110.

[17] Z. Zhai, B. Ren, Y. Xu, S. Wang, L. Zhang, Z. Liu, Nitrogen self-doped carbon aerogels from chitin for supercapacitors, J. Power Sources 481 (2021), 228976.

[18] M.S. Nazari, A.Noori Rahmanifar, W. Li, C. Zhang, M.F. Mousavi, The ordered mesoporous carbon nitride-graphene aerogel nanocomposite for high-performance supercapacitors, J. Power Sources 494 (2021), 229741.

[19] H. Wang, H. Niu, H. Wang, W. Wang, X. Jin, H. Wang, H. Zhou, T., Lin micro-meso porous structured carbon nanofibers with ultra-high surface area and large supercapacitor electrode, J. Power Sources 482 (2021), 228986.

[20] W. Chen, H. Wang, H. Lan, D. Li, A. Zhang, C. Liu, Construction of sugarcane bagasse-derived porous and flexible carbon nanofibers by electrospinning for supercapacitors, Ind Crops Prod 170 (2021), 113700.

[21] C.G. Real, R. Vicentini, W.G. Nunes, A.M. Pascon, F.A. Campos, L.M.Da Silva, R. G. Freitas, H. Zanin, Analyses of dispersive effects and the distributed capacitance in the time and frequency domains of activated carbon nanofiber electrodes as symmetric supercapacitors, Electrochim. Acta 402 (2022), 139299.

[22] Y. Liu, P. Liu, S. Wang, Z. Pan, C. Song, T. Wang, Fabrication of biomass-derived activated carbon with interconnected hierarchical architecture via H3PO4-assisted KOH activation for high-performance symmetrical supercapacitors, J. Electroanal. Chem. 903 (2021), 115828.

[23] T. Yumak, D. Bragg, E.M. Sabolsky, Effect of synthesis methods on the surface and electrochemical characteristics of metal oxide/activated carbon composites for supercapacitor applications, Appl. Surf. Sci. 469 (2019) 983–993.

[24] A. Apriwandi, E. Taer, R. Farma, R.N. Setiadi, E., Amiruddin a facile approach of micro-mesopores structure binder-free coin/monolith solid design activated carbon for electrode supercapacitor, J. Energy Storage 40 (2021), 102823.

[25] G.S. dos Reis, R.M.A.P. Lima, S.H. Larsson, C.M. Subramanaiyam, V.M. Dinh, M. Thyrel, H.P. de Oliveira, Flexible supercapacitors of biomass-based activated carbon-polypyrrole on eggshell membranes, J. Environ. Chem. Eng. 9 (2021), 106155.

[26] B.L. Vijayan, I.I. Misnon, G.M.A. Kumar, K. Miyajima, M.V. Reddy, K. Zaghib, C. Karuppiah, C.-C. Yang, R. Jose, Facile fabrication of thin metal oxide films on porous carbon for high density charge storage, J. Colloid Interface Sci. 562 (2020) 567–577.

[27] Y. Zhang, S.-J. Park, Incorporation of RuO2 into charcoal-derived carbon with controllable microporosity by CO2 activation for high-performance supercapacitor, Carbon 122 (2017) 287–297.

[28] B.L. Vijayan, I.I. Misnon, C. Karuppaiah, G.M.A. Kumar, S. Yang, C.-C. Yang, R. Jose, Thin metal film on porous carbon as a medium for electrochemical energy storage, J. Power Sources 489 (2021), 229522.

[29] B.L. Vijayan, I.I. Misnon, G.M. Anilkumar, C.-C. Yang, R. Jose, Void-size-matched hierarchical 3D titania flowers in porous carbon as an electrode for high-density supercapacitive charge storage, J. Alloys Compd. 858 (2021), 157649.

[30] I.M.A. Mohamed, A.S. Yasin, C. Liu, Synthesis, surface characterization and electrochemical performance of ZnO@activated carbon as a supercapacitor electrode material in acidic and alkaline electrolytes, Ceram. Int. 46 (2020) 3912–3920.

[31] K.S. Kim, S.J. Park, Bridge effect of silver nanoparticles on electrochemical performance of graphite nanofiber/polyaniline for supercapacitor, Synth. Met. 162 (2012) 2107–2111.

[32] M.Y. Bhat, N. Yadav, S.A. Hashmi, A high performance flexible gel polymer electrolyte incorporated with suberonitrile as additive for quasi-solid carbon supercapacitor, Mater. Sci. Eng. B. 262 (2020), 114721.

[33] C. Zhong, Y. Deng, W. Hu, D. Sun, X. Han, J. Qiao, J. Zhang, Electrolytes for Electro-chemical Supercapacitors, CRC Press, 2016.

[34] B. Pal, S. Yang, S. Ramesh, V. Thangadurai, R. Jose, Electrolyte selection for supercapacitive devices: a critical review, Nanoscale Adv. 1 (2019) 3807–3835.

[35] A. Gupta, A. Jain, S.K. Tripathi, Structural, electrical and electrochemical studies of ionic liquid-based polymer gel electrolyte using magnesium salt for supercapacitor application, J. Polym. Res. 28 (2021) 1–11.

[36] S.B. Aziz, A.S.F.M. Asnawi, R.T. Abdulwahid, H.O. Ghareeb, S.M. Alshehri, T. Ahamad, J.M. Hadi, M.F.Z. Kadir, Design of potassium ion conducting PVA based polymer electrolyte with improved ion transport properties for EDLC device application, J. Mater. Res. Technol 13 (2021) 933–946.

[37] S. Alipoori, M.M. Torkzadeh, S. Mazinani, S.H. Aboutalebi, F. Sharif, Performance-tuning of PVA-based gel electrolytes by acid/PVA ratio and PVA molecular weight, SN Appl. Sci. 3 (2021) 310.

[38] K. Sreekanth, T. Siddaiah, N.O. Gopal, Y.M. Kumar, C. Ramu, Optical and electrical conductivity studies of VO2+ doped polyvinyl pyrrolidone (PVP) polymer electrolytes, J. Sci. Adv. Mater. Dev. 4 (2019) 230–236.

[39] X. Liu, X. Xin, L. Shen, Z. Gu, J. Wu, X. Yao, Poly(methyl methacrylate)-based gel polymer electrolyte for high-performance solid state Li–O2 battery with enhanced cycling stability, ACS Appl. Energy Mater. 4 (2021) 3975–3982.

[40] A. Gupta, A. Jain, S.K. Tripathi, Structural and electrochemical studies of bromide derived ionic liquid-based gel polymer electrolyte for energy storage application, J. Energy Storage 32 (2020), 101723.

[41] J. Jie, Y. Liu, L. Cong, B. Zhang, W. Lu, X. Zhang, J. Liu, H. Xie, L. Sun, High-performance PVDF-HFP based gel polymer electrolyte with a safe solvent in Li metal polymer battery, J. Energy Chem. 49 (2020) 80–88.

[42] S.K. Tripathi, A. Jain, A. Gupta, M. Mishra, Electrical and electrochemical studies on magnesium ion-based polymer gel electrolytes, J. Solid State Electrochem 16 (2012) 1799–1806.

[43] V. Biju, N. Sugathan, V. Vrinda, S.L. Salini, Estimation of lattice strain in nanocrystalline silver from X-ray diffraction line broadening, J. Mater. Sci. 43 (2008) 1175–1179.

[44] M. Michalska, D.A. Buchberger, J.B. Jasiński, A.K. Thapa, A. Jain, Surface modification of nanocrystalline LiMn2O4 using graphene oxide flakes, Materials 14 (2021) 4134.

[45] A. Jain, S.K. Tripathi, Nano-porous activated carbon from sugarcane waste for supercapacitor application, J. Energy Storage 4 (2015) 121–127.

[46] S. Brunauer, L.S. Deming, W.E. Deming, E. Teller, On a theory of the van der Waals adsorption of gases, J. Am. Chem. Soc. 62 (1940) 1723–1732.

[47] H. Marsh, F. Rodriguez-Reinonso, Activated Carbon, Elsevier Science & Technology Books, Amsterdam, 2006.

[48] I.G. Inal, Z. Aktas, Enhancing the performance of activated carbon based scalable supercapacitors by heat treatment, Appl. Surf. Sci. 514 (2020), 145895.

[49] L.E. Helseth, Comparison of methods for finding the capacitance of a supercapacitor, J. Energy Storage 35 (2021), 102304.

[50] K.S. Lee, Y.J. Seo, H.T. Jeong, Capacitive behavior of functionalized activated carbon-based all-solid-state supercapacitor, Carbon Lett. 31 (2021) 1041–1049.

[51] J.R. Miller, Pulse power performance of electrochemical capacitors: technical status of present commercial devices, in: Proc. 8th International Seminar on Double Layer Capacitors and Similar Energy Storage Devices, Deerfield Beach Fla, Dec. 7-9, 1998.

[52] Md.Yasir Bhat, Nitish Yadav, S.A. Hashmi, Pinecone-derived porous activated carbon for high performance all-solid-state electrical double layer capacitors fabricated with flexible gel polymer electrolytes, Electrochim Acta 304 (2019) 94–108.

[53] J. Liu, Z. Khanam, S. Ahmed, H. Wang, T. Wang, S. Song, A study of low-temperature solid-state supercapacitors based on Al-ion conducting polymer electrolyte and graphene electrodes, J. Power Sources 488 (2021), 229461.

[54] Y.Jing Y. Liu, X. Chen, Z. Hu, G. Zhao, Carbon electrode material with high densities of energy and power, Acta Phys. - Chim. Sin. 24 (2008) 13–19.

[55] L. Xiao, X. Wei, Z. Shuping, Z. Lin, L. Feng, Q.S. Zhnag, G.Q. Lu, Preparation of capacitor's electrode from sunflower seed shell, Bioresour. Technol. 102 (2011) 1118–1123.

[56] J. Li, G. Zan, Q. Wu, Nitrogen and sulfur self-doped porous carbon from brussel sprouts as electrode materials for high stable supercapacitors, RSC Adv. 6 (2016) 57464–57472.

[57] F. Barzegar, A. Bello, J.K. Dangbegnon, N. Manyala, X. Xia, Asymmetric carbon supercapacitor with activated expanded graphite as cathode and Pinecone tree activated carbon as anode materials, Energy Procedia 105 (2017) 4098–4103.

[58] A. Bello, N. Manyala, F. Barzegar, A.A. Khaleed, Y. Damilola Momodua, J. K. Dangbegnona, Renewable pine cone biomass derived carbon materials for supercapacitor application, RSC Adv 6 (2016) 1800–1809.